Computational Study of the Reaction of Chlorinated Vinyl Radical with Molecular Oxygen ($C_2Cl_3 + O_2$)

Huan Wang,[†] Jicun Li,[‡] Xinli Song,[‡] Yuzhen Li,[‡] Hua Hou,[‡] Baoshan Wang,*[,‡] Hongmei Su,*[,†] and Fanao Kong[†]

College of Chemistry and Molecular Sciences, Wuhan University, Wuhan 430072, and Institute of Chemistry, Chinese Academic Society, Beijing 100080, P. R. China

Received: May 30, 2006; In Final Form: July 12, 2006

Eight exothermic product channels of the reaction of chlorinated vinyl radical (C_2Cl_3) with molecular oxygen (O_2) have been investigated using ab initio quantum chemistry methods. The energetics of the reaction pathways were calculated at the second-order Moller−Plesset Gaussian-3 level of theory (G3MP2) using the B3LYP/6-311G(d) optimized geometries. It has been shown that the $C_2Cl_3 + O_2$ reaction takes place via a barrierless addition to form the chlorinated vinylperoxy radical complex, which can decompose or isomerize to various products via the complicated mechanisms. Two major reaction routes were revealed, i.e., the three-member-ring reaction mechanism leading to $ClCO + CCl_2O$, $CO + CCl_3O$, $CO_2 + CCl_3$, $Cl + (ClCO)_2$, etc., and the OO bond cleavage mechanism leading to $O(^3P) + C_2Cl_3O$. The other mechanisms are shown to be unimportant. The results are validated by the calculations using the restricted coupled cluster theory [RCCSD(T)] with the complete basis set extrapolation. Variational transition state theory was employed to calculate the individual and total rate coefficients as a function of temperature and pressure (helium). The theoretical rate coefficients are in good agreement with the available experimental data. It was found that the total rate coefficients show strong negative temperature dependence in the range 200−2000 K. At room temperature (297 K), the total rate coefficients are shown to be nearly pressure independent over a wide range of helium pressures ($1-10^9$ Torr). The deactivation of the initial adduct, $C_2Cl_3O_2$, is only significant at pressures higher than 1000 Torr. The three-member-ring reaction mechanism is always predominant over the OO bond cleavage.

I. Introduction

The oxidation of chlorinated hydrocarbons is involved in many practical processes, for example, the soot formation in flames and the combustion of chlorinated hydrocarbons.[1,2] It is well-known that the vinyl radicals (C_2H_3) play important roles in the formation of aromatics, soot, and coke in hydrocarbon pyrolysis.[3] The presence of O_2 is capable of suppressing such unwanted processes in combustion by its competing fast and highly exothermic reaction with vinyl radicals. In contrast, the reaction of chlorinated vinyl with oxygen has not been well understood up to date.

The kinetics of the $C_2Cl_3 + O_2$ reaction were studied by Russell, Seetula, Gutman, and Senkan (RSGS)[4] in 1989 using a tubular flow tube reactor coupled with a photoionization mass spectrometer in the temperature range 298−648 K. C_2Cl_3 was generated by laser photolysis of C_2Cl_4. It was shown that the $C_2Cl_3 + O_2$ reaction is fast and exhibits negative temperature dependence, e.g., $k = 2 \times 10^{-12} \exp(418/T)$ $cm^3molecule^{-1}s^{-1}$. No pressure dependence was observed in helium bath gas. The products of the reaction have not been detected.

Recently, Su and co-workers studied the $C_2Cl_3 + O_2$ reaction by time-resolved FTIR spectroscopy at room temperature.[5] Strong infrared emission signals due to $CO(v \rightarrow v - 1, v = 1-10)$ and $CO_2(v \rightarrow v - 1, v_3 = 1-10)$ were observed. This experiment indicates that there are quite complicated multistep mechanisms in the $C_2Cl_3 + O_2$ reaction because the molecule structures of the observed products have nothing in common with those of the reactants.

Ab initio calculation is very helpful to clarify the detailed reaction mechanisms. By exploring all the possible intermediates and transition states, the minimum energy reaction paths for every energetically accessible product channels can be obtained. Moreover, if the reaction system exhibits the statistical behavior, the kinetics, e.g., the rate coefficients and branching ratios, can be deduced readily using the transition state theory and multichannel RRKM theory.

In this paper, the energetics of the reaction pathways for the $C_2Cl_3 + O_2$ reaction has been investigated using various ab initio methods. The mechanisms for the following exothermic product channels are revealed for the first time, viz.:

$$C_2Cl_3 + O_2 \rightarrow ClCO \text{ (carbonyl chloride)} + CCl_2O \text{ (phosgene)} \quad (1)$$

$$\rightarrow O(^3P) + C_2Cl_3O \quad (2)$$

$$\rightarrow CO_2 + CCl_3 \quad (3)$$

$$\rightarrow CO + CCl_3O \quad (4)$$

$$\rightarrow Cl + (ClCO)_2 \text{ (oxalyl chloride)} \quad (5)$$

$$\rightarrow Cl + CCl_2C(O)O \text{ (chlorinated } \alpha\text{-lactone)} \quad (6)$$

$$\rightarrow CCl_2 + ClCO_2 \quad (7)$$

$$\rightarrow ClO + CCl_2CO \text{ (chlorinated ketene)} \quad (8)$$

* Corresponding author. E-mail: wangb@chem.whu.edu.cn.
[†] Chinese Academic Society.
[‡] Wuhan University.

10.1021/jp0633345 CCC: $33.50
Published on Web 08/05/2006

The other channels such as $ClO_2 + C_2Cl_2$ and $ClO + C_2Cl_2O$ are discarded because of their high endothermicities. Moreover, the temperature- and pressure-dependent rate coefficients for the overall reaction and for the most important two product channels (1) and (2) are calculated statistically in a temperature range 200−2000 K. Theoretical kinetic data are in good agreement with the available experimental data.[4] The experimentally observable products are suggested on the basis of the present ab initio energetics of the reaction pathways.

II. Computational Methods

The geometries of the reactants, products, various intermediates, and transition states were optimized using the hybrid density functional theory, i.e., Becke's three-parameter nonlocal exchange functional with the nonlocal correlation functional of Lee, Yang, Parr (B3LYP)[6] with the standard 6-311G(d) basis sets. For the current reaction involving seven heavy atoms, the B3LYP/6-311G(d) level of theory is a balanced method in the consideration of computational efficiency and accuracy. Moreover, the B3LYP/6-311G(d) level of theory is able to suppress effectively the problem of spin contaminant.

Harmonic vibrational frequencies and then the zero-point energies (ZPE) were calculated at the B3LYP/6-311G(d) level with the optimized geometries. The intermediates were characterized by all the real frequencies. The transition state has only one imaginary frequency. Connections of the transition states between two local minima have been confirmed by intrinsic reaction coordinate (IRC)[7] calculations at the B3LYP/6-311G(d) level.

The energies of the stationary points were calculated using the G3MP2 method,[8] which is a composite scheme based on three single-point energies, i.e., QCISD(T)/6-31G(d), MP2/6-31G(d), and MP2/g3mp2large. Higher-level corrections were made according to the numbers of α and β valence electrons (N_α, N_β). The G3MP2 total energy was obtained using the following formula:

$$E(\text{G3MP2}) = E[\text{QCISD(T)/6-31G(d)}] + E[\text{MP2/g3mp2large}] - E[\text{MP2/6-31G(d)}] + E(\text{HLC}) + E(\text{SO}) + E(\text{ZPE})$$

where $E(\text{HLC}) = -0.004995N_\alpha - 0.005046N_\beta$; the experimental spin−orbital (SO) corrections were used for atomic species (e.g., O, Cl); the B3LYP/6-311G(d) calculated ZPEs were used directly without scaling because empirically it appears that the ZPE at such a level of theory is in good agreement with the experimental values.

Meanwhile, the coupled cluster theory[9] was employed to investigate the most important reaction paths as shown below. The geometries were optimized at the CCSD level[10] with Dunning's correlation consistent basis set, cc-pVDZ.[11] The energies were calculated using the restricted coupled cluster theory with single, double, and noniterative triple excitations [RCCSD(T)] with the restricted open-shell Hartree−Fock references (ROHF).[12] Using the restricted wave function can eliminate the problem of spin contaminant involved in the present doublet state. The total energies were obtained using the complete basis set (CBS) extrapolation, i.e.,[13]

$$E(\text{CBS}) = E_{\text{HF}}(\text{CBS}) + \Delta E_{\text{corr}}(\text{CBS})$$

$$E_{\text{HF}}(\text{CBS}) = E_{\text{HF}}(X) + a\exp(-bX), \quad X = 2, 3, 4$$

$$\Delta E_{\text{corr}}(\text{CBS}) = \Delta E_{\text{corr}}(X) + cX^{-3}, \quad X = 3, 4$$

where a, b, and c are parameters and $X = 2$, 3, 4 for the cc-pVDZ, cc-pVTZ, and cc-pVQZ basis sets, respectively. The calculations at the RCCSD(T)/CBS level of theory not only represent the "best estimate" to the energetic data but also can be used to calibrate the empirical G3MP2//B3LYP data and thus to check the accuracy of such a level of theory.

It has been suggested that the tighter d functions besides the regular cc-pVXZ basis sets, i.e., cc-pV(X+d)Z, should be used for the Cl-containing molecules.[14] In the $C_2Cl_3 + O_2$ reaction, the Cl atoms do not participate directly to the reaction coordinates for those dominant mechanisms. Therefore, the regular cc-pVXZ basis sets should be reliable as well.

All the ab initio calculations were carried out using the Gaussian03[15] and Molpro programs.[16]

III. Results and Discussion

The calculated reaction pathways are shown in Figure 1. The corresponding structures and energies are summarized in Figures 2−3 and Table 1. Before the details of the reaction paths are discussed, it is worth presenting some arguments on the reliability and quality of the present ab initio calculations.

1. Validation of the Computational Schemes. One potential problem is that the high-level ab initio energies have been calculated on the basis of the lower-level optimized geometries, i.e., B3LYP/6−311(d). The geometries may change with the levels of theory used in the optimizations, and thus, the energetics can be affected significantly. Ideally, the geometries of the stationary points should be calculated at high level of theory as well rather than B3LYP/6-311G(d). For example, the QCISD(T)/g3mp2large level of theory, which is identical to the G3MP2 method, is one of the choices. We cannot afford such demanding calculations for the present $C_2Cl_3O_2$ system including seven heavy atoms. Fortunately, the influence of the geometrical changes on the energetics appears to be a systematic error. As shown in Figure 4, in comparison of the energies obtained at the G3MP2 and B3LYP/6-311G(d) levels for all the stationary points found in the $C_2Cl_3 + O_2$ reaction, there is a very good linear correlation between the two sets of data. The slope of the least-squares fitted line is 0.99, which is essentially one, and the offset is −28 kJ/mol. This indicates that the B3LYP/6-311G(d) calculated energies are systematically higher than the G3MP2 energies by 28 kJ/mol. To some extent, this comparison implies that the B3LYP/6-311G(d) optimized geometries are reliable and the energies are not sensitive to the changes of the geometrical parameters. Meanwhile, the calculated reaction heats are in good agreement with the experimental data, as shown in Table 1.

It is worthy of comparing the geometries and energies calculated at the G3MP2//B3LYP level with those at the RCCSD(T)/CBS//CCSD level. The latter is considered to be our best estimates to the energetics of the reaction pathways. Only the most important stationary points have been calculated at the RCCSD(T)/CBS//CCSD level of theory, including IM1t, IM2, IM4, TS1, TS2, TS3, TS4, and TS18. As shown in Figures 2 and 3, the B3LYP/6-311G(d) and CCSD/cc-pVDZ geometrical parameters of these eight structures are in good agreement except for the distance of the breaking OO bond of TS3. The CCSD/cc-pVDZ method gives much longer OO distance for TS3. In view of the energies, with respect to the reactants ($C_2Cl_3 + O_2$) asymptote, the RCCSD(T)/CBS data are generally higher than the G3MP2 energies by about 5−10 kJ/mol (see Table 1), which are comparative with the error bars of the calculated energies. However, the energy of TS2 becomes lower by 11 kJ/mol. The significance of such a change is that the energy difference

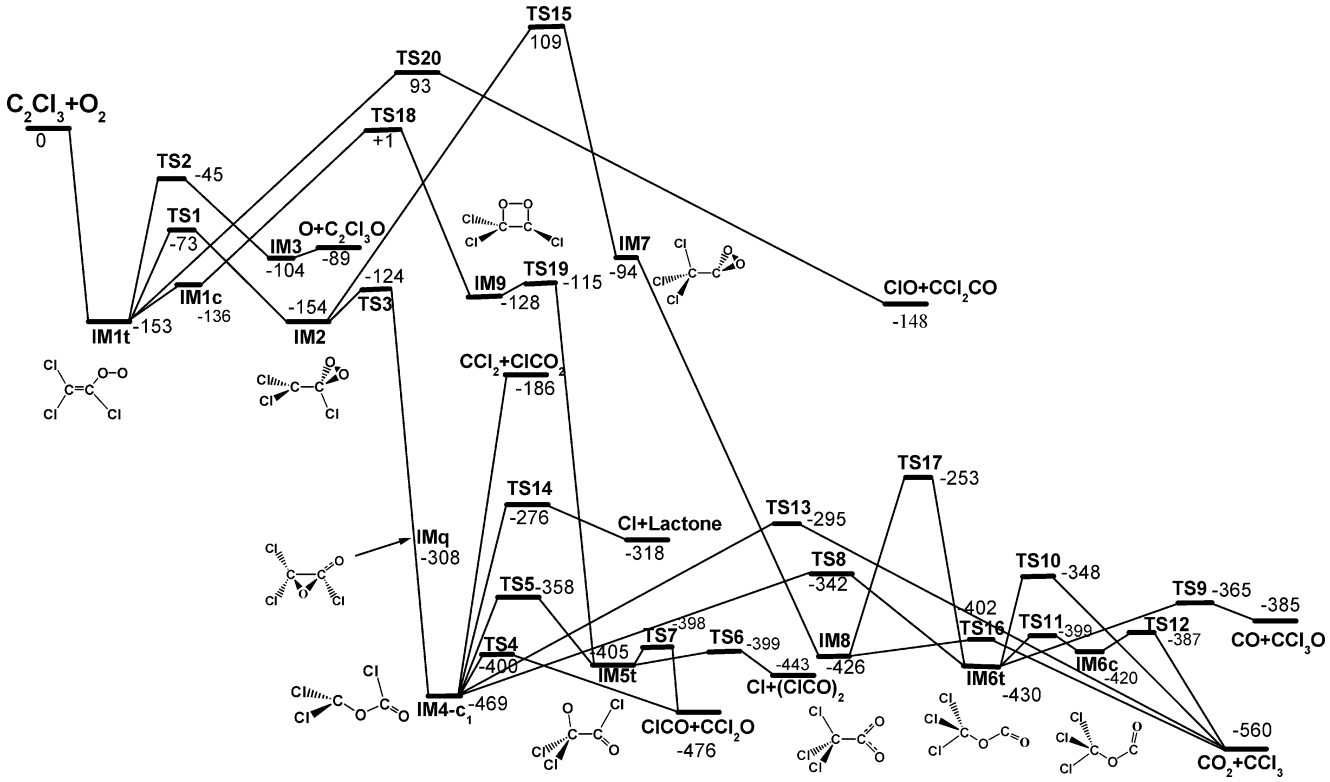

Figure 1. Profiles of the potential energy surface for the $C_2Cl_3 + O_2$ reaction. The indicated energies (in kJ/mol) are obtained at the G3MP2//B3LYP/6-311G(d) level of theory.

between TS1 and TS2, which are two key transition states, is reduced to 6 kJ/mol from the G3MP2 predicted 28 kJ/mol. Evidently, the branching ratios for the two channels will be significantly affected. This issue will be addressed in details in the following kinetic calculations. Interestingly, the energy of TS3 is only slightly lowered at the RCCSD(T)/CBS level, although the geometries of TS3 changes apparently from B3LYP/6-311G(d,p) to CCSD/cc-pVDZ.

In short, the use of the G3MP2//B3LYP/6-311G(d) level of theory to study the $C_2Cl_3 + O_2$ reaction is reasonable in view of the relative importance of various product channels. The basic feature of the reaction pathways should be qualitatively good enough although the absolute yields of the product channels might be uncertain.

We have not performed any multireference self-consistent-field and configuration interaction (MCSCF or MRCI) calculations for the $C_2Cl_3 + O_2$ reaction. While the complete active space (e.g., 41 electrons in 28 valence orbitals) calculation cannot be afforded, the calculations using smaller space and basis sets are less meaningful because this kind of calculation is sensitive to the sizes of both the active spaces and the basis sets. However, it has been shown that the multireference treatment of the wave function is *NOT* critical for the analogous $C_2H_3 + O_2$ reaction.[17] Both G3MP2 and RCCSD(T)/CBS methods can give good energetic data which are in agreement with the results obtained by the multireference configuration interaction theory.

In the following section, the reaction mechanism will be discussed on the basis of the geometrical evolutions. The G3MP2//B3LYP/6-311G(d) data will be used in the discussion unless stated otherwise.

2. Reaction Mechanism. The $C_2Cl_3 + O_2$ reaction starts by the formation of the chlorinated vinylperoxy radical $C_2Cl_3O_2$. Depending on the orientation of the initial attack of O_2, i.e., the dihedral angle of OOCC, $C_2Cl_3O_2$ can be in trans (IM1t) or cis (IM1c) conformations. However, IM1c is shown to be a transition state corresponding to the internal rotation around the newly formed CO bond. In view of the bond lengths, the CC bond keeps to be a double bond. Both CO and OO are single bonds. Therefore, the radical site shifts from C_2Cl_3 to the terminal O atom of $C_2Cl_3O_2$ after addition. The energy of IM1t is 153 kJ/mol lower than that of the reactants.

The reaction proceeds via decomposition or isomerization of the energized IM1t. The energetically most favorable route is forming a three-member-ring COO structure (IM2) via transition state TS1. Although the strong strain might exist for such a structure, the energy of IM2 is almost identical to that of IM1t. Both IM2 and IM1t have C_s symmetry, but IM2 has $^2A'$ electronic state and IM1t is in $^2A''$ state. During the reaction, the OO bond is stretched by about 0.14 Å, and simultaneously, the terminal O atom is moved toward the C atom by decreasing the COO angle from 116.6 to 83.2°. The newly formed CO bond is 1.859 Å. The barrier height is 80 kJ/mol with respect to IM1t.

The simple OO bond cleavage of IM1t occurs via transition state TS2, forming the products $O(^3P)$ and C_2Cl_3O radical. The breaking OO bond is elongated from 1.322 to 1.756 Å. TS2 has no symmetry. The leaving O atom is almost nearly perpendicular to the CCO plane of the final planar C_2Cl_3O product. The barrier height for TS2 is uncertain; it varies from 108 kJ/mol at the G3MP2 level to 87 kJ/mol at the RCCSD(T)/CBS level. Because there is severe spin contaminant in the unrestricted wave functions for TS2, the RCCSD(T)/CBS value should be more reliable. It is noted that there is a well in the product side, denoted as IM3. The long-range interaction between $O(^3P)$ and C_2Cl_3O leads to this complex. The OO distance is as long as 2.738 Å. The binding energy of IM3 is 15 kJ/mol with respect to $O(^3P) + C_2Cl_3O$.

In comparison with the three-center isomerization of IM1t to IM2, there is a four-center isomerization route leading to the

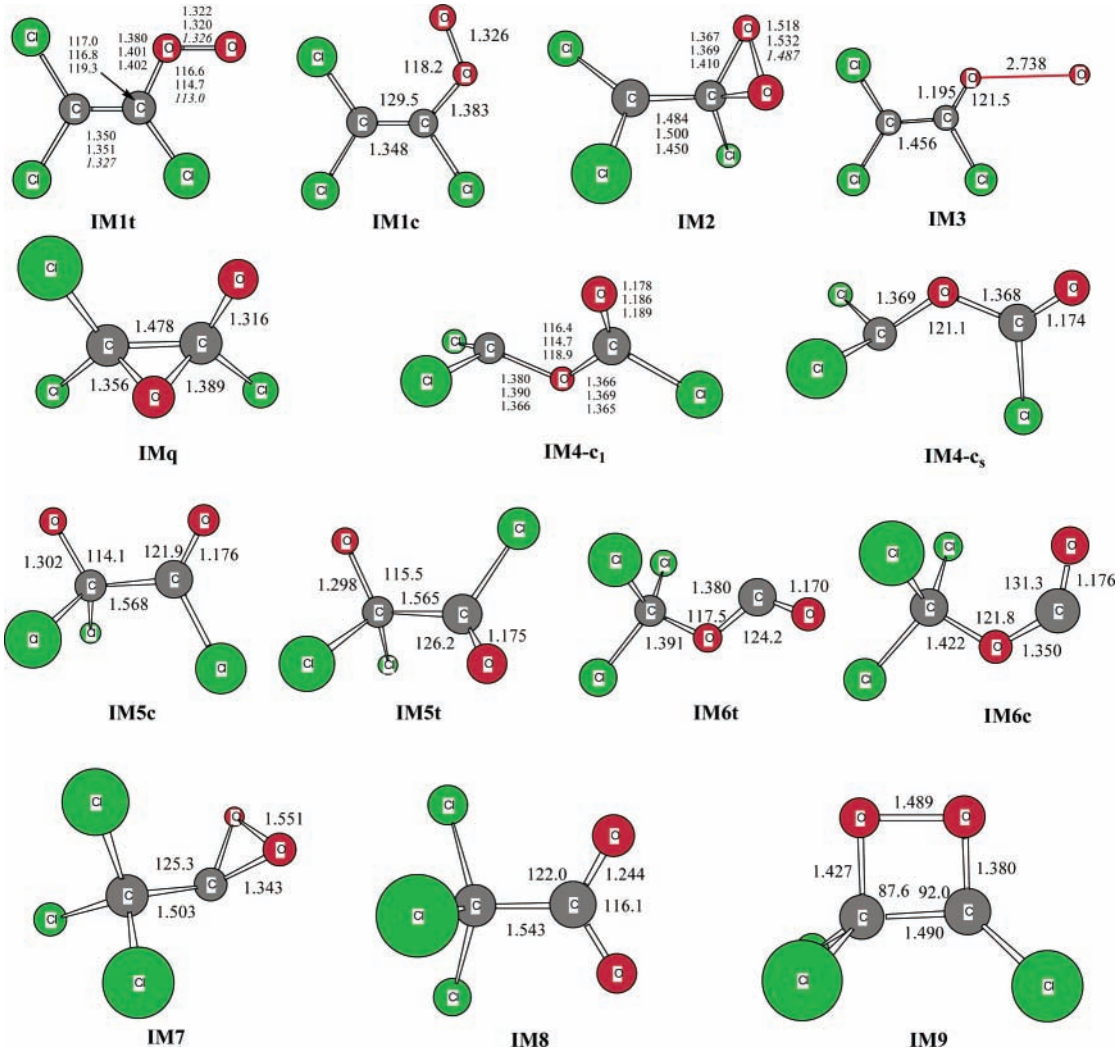

Figure 2. Structures of the intermediates involved in the $C_2Cl_3 + O_2$ reaction. Selected geometrical parameters obtained at the B3LYP/6-311G(d) level are shown. For IM1t, IM2, and IM4-c_1, the second entries are the parameters at the CCSD/cc-pVDZ level and the third entries correspond to the geometrical parameters for the analogous species involved in the $C_2H_3 + O_2$ reaction (see ref 17). Note that the geometry of IMq can be only optimized at the HF/6-311G(d) level. Bond distances are in angstroms and bond angles are in degrees.

intermediate IM9 via IM1c and transition state TS18. The terminal O atom of IM1c approaches to the C atom. The OO bond is stretched slightly, and the forming OC bond is close to 2 Å. Meanwhile, the CC bond is stretched and its double bond feature disappears. In IM9, the four-member-ring CCOO is nearly in the plane. The isolated CCl bond is pointed out of the plane, and thus, IM9 has no symmetry. The barrier height for TS18 is 154 kJ/mol. Note that the energy of TS18 is very close to that of the reactants. IM9 lies about 25 kJ/mol above IM1t and IM2.

It has been suggested by RSGS that the formation of ClO and CCl_2CO is a possible product channel in the $C_2Cl_3 + O_2$ reaction.[4] A transition state for this process was located to be TS20. Evidently, this is a 4-center ClO elimination path. The barrier for TS20 is as high as 246 kJ/mol, making this barrier lie well above the reactants $C_2Cl_3 + O_2$. Therefore, this mechanism can be excluded theoretically.

It is interesting to note that for the $C_2Cl_3O_2$ peroxy radical, the 3-center isomerization involves a lower barrier than the 4-center isomerization and 4-center elimination. In other words, the 3-center reaction is more favorable than the 4-center reaction, even though the former is supposed to have larger strain and thus is less stable.

The subsequent reactions starting from IM2 and IM9 were also investigated to gain insight into the productions of small fragments. The OO bond of IM2 is fairly weak. The breaking of OO bond takes place via transition state TS3, which is a low barrier (ca. 30 kJ/mol). Compared with IM2, the OO distance of TS3 is stretched by about 15%. Very interestingly, one of O atoms tends to attack the CC bond via an intermediate IMq, and subsequently, the O atom is inserted into the CC bond and the CC bond is broken simultaneously. IMq involves a three-center CCO structure but it is a transient, quasistable species because it only exists at the lower levels of theory [e.g., HF/6-311G(d)] and it disappears even at the B3LYP/6-31G(d) level. The final intermediate generated via the above concerted bond cleavage and intramolecular insertion mechanism is IM4. As shown in Figure 1, IM4 represents the global minimum on the potential energy surface. IM4 can be either symmetrical (IM4-c_s) or unsymmetrical (IM4-c_1) whereas the former is slightly higher in energy. There is a great amount of available energy (469 kJ/mol) deposited into IM4, and thus, many product channels are open starting from IM4.

The most favorable dissociation channel of IM4 is the production of ClCO and CCl_2O via transition state TS4. This is a simple CO bond fission process. The barrier height is 69 kJ/mol with respect to IM4. The formation of ClCO + CCl_2O is highly exothermic. It is conceivable that both ClCO radical and CCl_2O molecule can be produced in their highly vibrationally excited

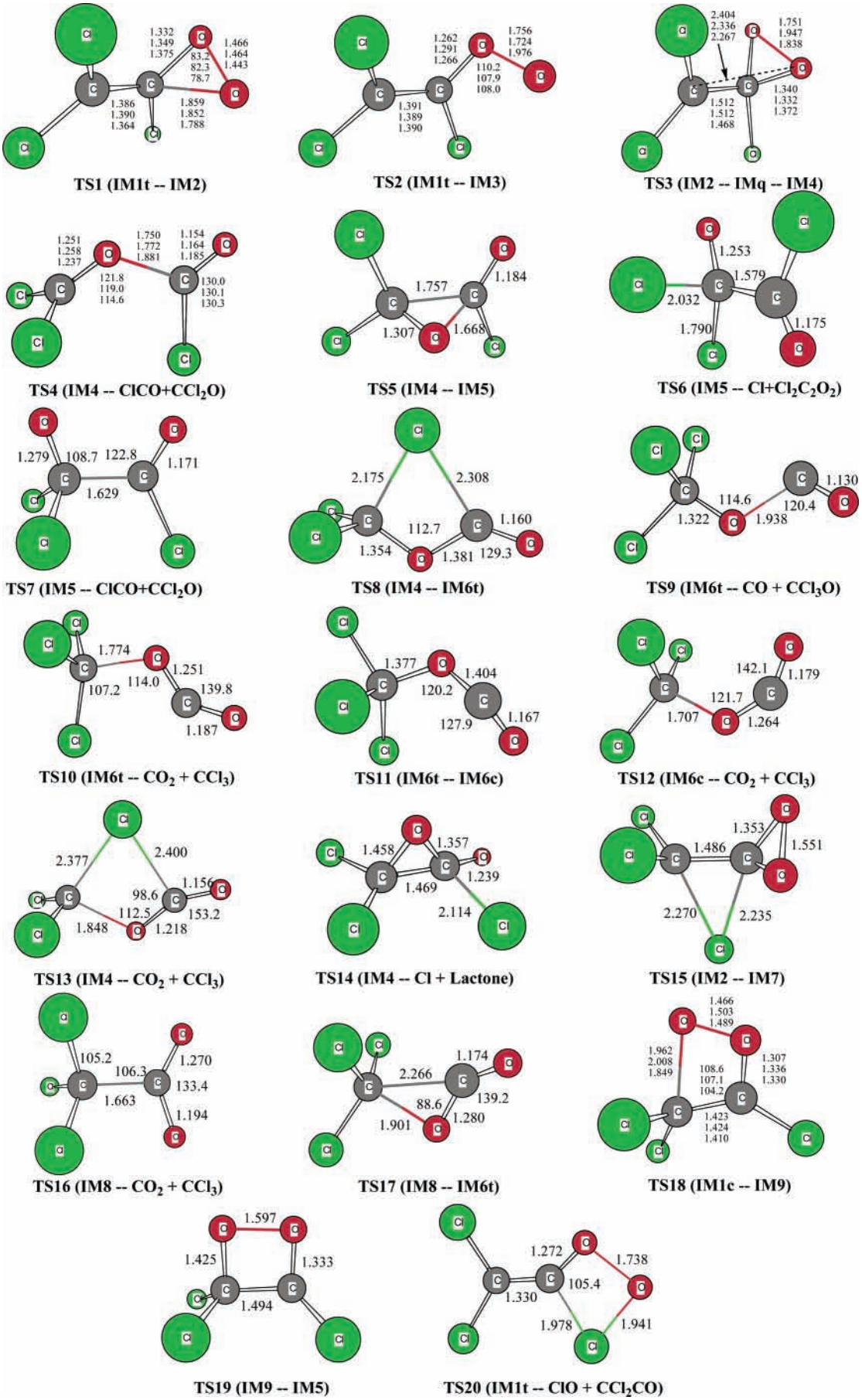

Figure 3. Structures of the transition states involved in the $C_2Cl_3 + O_2$ reaction. Selected geometrical parameters obtained at the B3LYP/6-311G-(d) level are shown. For TS1, TS2, TS3, TS4, and TS18, the second entries are the parameters at the CCSD/cc-pVDZ level and the third entries correspond to the geometrical parameters for the analogous species involved in the $C_2H_3 + O_2$ reaction (see ref 17). Bond distances are in angstroms and bond angles are in degrees.

TABLE 1. B3LYP/6-311G(d) Calculated Zero-Point Energies (ZPE, in kJ/mol) and the Relative Energies (ΔE, in kJ/mol) at Various Levels of Theory (with ZPE Corrections)

species	ZPE	ΔE (B3LYP)	ΔE (G3MP2)	ΔE (CBS)[a]	ΔE (exptl)[b]
$C_2Cl_3 + O_2$	42	0	0	0	
IM1t	52	−126	−153	−143 [−184]	
IM1c	51	−108	−136		
IM2	51	−106	−154	−149 [−146]	
IM3	45	−73	−104		
IM4-c_s	54	−432	−462		
IM4-c_1	55	−437	−469	−465	
IM5t	50	−386	−405		
IM5c	51	−378	−402		
IM6t	52	−386	−430		
IM6c	52	−375	−420		
IM7	50	−39	−94		
IM8	51	−394	−426		
IM9	53	−85	−128		
TS1	47	−48	−73	−62 [−82]	
TS2	45	−44	−45	−56 [−28]	
TS3	46	−78	−124	−129 [−74]	
TS4	46	−391	−400	−392	
TS5	49	−325	−358		
TS6	49	−382	−399		
TS7	47	−377	−398		
TS8	49	−324	−342		
TS9	44	−345	−365		
TS10	47	−315	−348		
TS11	50	−355	−399		
TS12	48	−356	−387		
TS13	47	−300	−295		
TS14	49	−251	−276		
TS15	44	108	109		
TS16	47	−373	−402		
TS17	43	−213	−253		
TS18	48	11	1	−2	
TS19	47	−81	−115		
TS20	44	134	93		
$ClCO + CCl_2O$	44	−469	−476		−473
$O(^3P) + C_2Cl_3O$	44	−70	−89		−80
$CO_2 + CCl_3$	49	−540	−560		−550
$CO + CCl_3O$	39	−360	−385		−382
$Cl + (ClCO)_2$	52	−437	−443		−442
Cl + α-lactone	51	−299	−318		
$ClO + CCl_2CO$	45	−127	−148		
$CCl_2 + ClCO_2$	37	−182	−186		

[a] The data in brackets correspond to the energies for the $C_2H_3 + O_2$ reaction obtained at the RCCSD(T)/CBS level in ref 17b. [b] The experimental reaction energies are obtained using the enthalpies of formation of the species in NIST webbook (http://webbook.nist.gov/chemistry/).

states. Secondary reactions such as the direction decomposition of ClCO → Cl + CO and the reaction between ClCO and O_2 might take place readily. The details for these secondary reactions will be reported elsewhere.

The second reaction path of IM4 is the isomerization to another intermediate IM5 via transition state TS5. It should not be confused with the analogous structure of IMq, although TS5 involves a three-member-ring structure as well. In fact, TS5 represents a ClCO migration transition state. The C atom of the ClCO moiety shifts from O atom to C atom with the concerted CO bond breaking and CC bond forming. The normal mode of the imaginary frequency of TS5 and the IRC calculation confirms the connection of TS5 with IM4 and IM5. The barrier height is 111 kJ/mol, which is 42 kJ/mol higher than that for TS4. Depending on the OCCO dihedral angle, there are trans and cis conformers for IM5. Their energies are almost the same. IM5 is very unstable. It can decompose to form Cl atom and $(ClCO)_2$ via the simple CCl bond cleavage (TS6) or to form

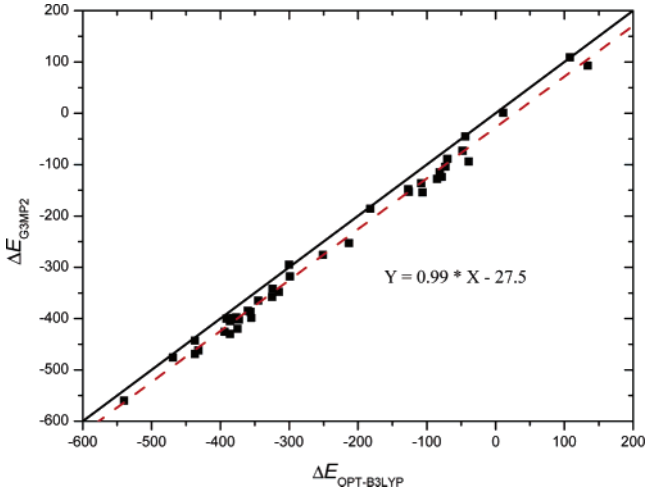

Figure 4. Comparison of the B3LYP/6-311G(d,p) energies ($\Delta E_{opt-B3LYP}$) with those calculated at the G3MP2 level using the B3LYP/6-311G(d) optimized geometries (ΔE_{G3MP2}). All the relative energies including barrier heights and reaction heats with respect to the $C_2Cl_3 + O_2$ asymptote are included. The *x* and *y* axes have the same scales (in kJ/mol) as indicated by the diagonal line. The linear fit of all the data are shown as the dashed line.

$ClCO + CCl_2O$ by slightly stretching of the CC bond (TS7). The decomposition barriers are only 6−7 kJ/mol.

Special attention was paid to the CO and CO_2 productions in the $C_2Cl_3 + O_2$ reaction. Note that the $CO_2 + CCl_3$ channel is the most exothermic channel in the title reaction. A few reaction paths leading to CO and CO_2 have been investigated. A direct production channel of CO_2 was found. The corresponding transition state is TS13, which is a four-center CO_2 elimination structure. Its barrier height is 174 kJ/mol. The lower barrier channels do exist but another intermediate CCl_3OCO (IM6) is involved. There are two stable conformers for IM6, namely, trans and cis forms, where the trans CCl_3OCO (IM6t) is obtained via the Cl migration of IM4. The relevant transition state is denoted as TS8. The barrier height for TS8 is about 47 kJ/mol lower than that for TS13. In comparison of the geometries of TS8 and TS13, the only obvious difference is that the CO bond of TS13 is elongated but that of TS8 almost keep unchanged. IM6t may decompose by breaking the two OC single bonds, forming $CO + CCl_3O$ via TS9 or $CO_2 + CCl_3$ via TS10, respectively. The energy of TS10 is 17 kJ/mol higher than that of TS9. Additionally, there is an alternative path for the $CO_2 + CCl_3$ channel, i.e., the cis CCl_3OCO (IM6c) is formed first via an internal rotation transition state TS11 and then the CO bond cleavage leads to CO_2 and CCl_3 via TS12. Interestingly, the barrier for TS12 is significantly lower than that for TS10, which indicates that the CO_2 elimination from the cis CCl_3OCO conformer is more favorable than that from the trans conformer. Such an anisotropic reaction does not occur for the $CO + CCl_3O$ channel because no true transition state can be found for IM6c → $CO + CCl_3O$.

The last two channels considered involve significant barriers with respect to IM4. One is the Cl elimination to form chlorinated α-lactone via transition state TS14. The other path leads to CCl_2(singlet) and $ClCO_2$ without any additional barrier. It is noted that both lactone and $ClCO_2$ can decompose into CO_2 molecules quickly.

It should be mentioned that all the barriers involved in the reaction paths discussed above starting from IM4 are far below the energy of the reactants ($C_2Cl_3 + O2$). Therefore, these reactions can undergo readily in the consideration of the huge available energy of IM4.

For completeness, two more reaction paths have been investigated. One of them is the Cl migration of IM2 to form the intermediate IM7 via TS15. The COO three-member-ring structure keeps unchanged during the Cl migration. IM7 is a quasistable species because the OO bond is breaking without any barrier to form another low energy intermediate IM8. As long as the CC bond of IM8 is slightly stretched, it can decompose to $CO_2 + CCl_3$ via a minor barrier TS16 (24 kJ/mol). Of course, IM8 can isomerize to IM6t via a CCl_3 migration transition state TS17 but the barrier height is much higher. However, this mechanism for CO_2 production is negligible because the rate-determining TS15 lies about 109 kJ/mol above the reactants. The other reaction is the isomerization between IM9 and IM5 via TS19. This is an open-ring process. TS19 is an early barrier as indicated by the slightly stretched OO distance. In comparison with the preceding ring-forming transition state TS18, the barrier for TS19 is only 13 kJ/mol, which is less than 10% of that for TS18. Therefore, this might be a potential channel for the $ClCO + CCl_2O$ production, but the rate-determining barrier (TS18) is too high to be important.

In summary, there are two major reaction paths revealed in the above discussions from the energetic point of view, namely,

$$C_2Cl_3 + O_2 \rightarrow IM1t \rightarrow TS1 \rightarrow IM2 \rightarrow TS3 \rightarrow IM4 \rightarrow TS4 \rightarrow ClCO + CCl_2O \quad \text{(Ch1)}$$

$$C_2Cl_3 + O_2 \rightarrow IM1t \rightarrow TS2 \rightarrow IM3 \rightarrow O(^3P) + C_2Cl_3O \quad \text{(Ch2)}$$

Both channels are exothermic, and all the barriers are well below the reactants. It should be confident that $ClCO + CCl_2O$ and $O(^3P) + C_2Cl_3O$ are the nascent products of the reaction of C_2Cl_3 with O_2. However, the production of CO and CO_2 cannot be ruled out. As shown in Figure 1, the key intermediate IM4 has so much available energy that its decomposition reactions might not occur statistically. The barriers leading to CO and CO_2 are very low in comparison with the available energy to IM4. In other words, these barriers are not critical anymore in the determination of the relative yields of the final products. This kind of nonstatistical dynamic behavior has been observed in many highly exothermic radical reactions where the products are generated just like from a direct reaction although there are intermediates and barriers along the minimum energy reaction paths.[18]

No matter how complicated the reaction mechanisms are, it is reasonable to assume that the following simplified reaction scheme represents the dominant mechanisms, viz.:

$$C_2Cl_3 + O_2 \rightleftarrows IM1t \xrightarrow{TS1} \text{products (ClCO, Cl, CO, } CO_2\text{, etc.)} \quad \text{(channel 1)}$$

$$\xrightarrow{TS2} O(^3P) + C_2Cl_3O \quad \text{(channel 2)}$$

Because the exothermicity of 153 kJ/mol for the formation of IM1t is a medium amount and the barriers TS1 and TS2 are more than 60 kJ/mol higher than IM1t, it is also reasonable to assume that the above reaction proceeds statistically. Therefore, the transition state theory and RRKM theory together with the master equation technique have been used to treat the kinetics of the reaction as detailed below.

3. Reaction Kinetics. Because there is no apparent barrier for the association of C_2Cl_3 with O_2, variational transition state theory was employed to treat the reaction entrance. It is noted that the locations of the variational transition states are temperature dependent. The potential energy surface for the entrance was constructed semiempirically. The reacting CO distance was set to be the variational reaction coordinate and was scanned from 1.6 to 3.2 Å with the step size of 0.1 Å, and simultaneously, the remaining geometrical parameters were optimized. To account for the anisotropic effect of the binding potential, an anisotropic potential form was adopted and the exponent of the angular dependence function is set to 2. Moreover, the pairwise Lennard-Jones (12-6) potentials, which describe the interactions between the atoms except the binding C and O atoms, have been added to the total interaction energy. The Lennard-Jones parameters are $\epsilon = 0.17, 0.17, 1.0$ kJ/mol and $\sigma = 3.2, 3.2, 3.4$ Å for C, O, Cl, respectively. Using the above potentials, the number of states along the reaction coordinate was calculated variationally at the energy and angular momentum (E/J) resolved level using the flexible transition state theory as implemented in the Variflex program.[19] As for the IM1t complex and the transition states TS1 and TS2, the rigid rotor harmonic oscillator approximation was employed to evaluate the number of states and the density of states. The minor tunneling effect due to TS1 and TS2 was considered using the Eckart model. The temperature and pressure dependence of the rate coefficients have been calculated using the one-dimensional master equation method. To compare the theoretical rate coefficients with the experimental data, helium was used as the bath gas. A simple exponential down energy transfer model was used for the IM1t−He collisions with the parameter $\alpha = 100$ cm^{-1}. Usually helium is not an efficient quencher, so the small arbitrary α value may be a reasonable estimate.

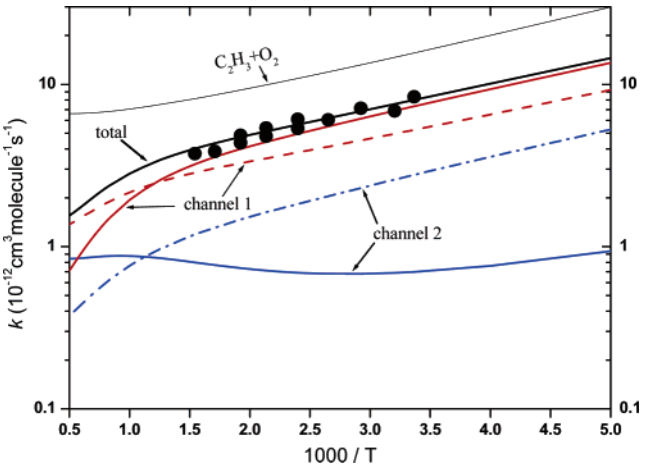

Figure 5. Temperature dependence of the calculated total rate coefficients and the individual rate coefficients for the channel 1: $C_2Cl_3 + O_2 \rightleftarrows IM1t \xrightarrow{TS1}$ products (ClCO, Cl, CO, CO_2, etc.) and channel 2: $C_2Cl_3 + O_2 \rightleftarrows IM1t \xrightarrow{TS2} O(^3P) + C_2Cl_3O$ with 2 Torr helium. The dots represent the experimental values of the total rate coefficients reported in ref 4. The solid lines are obtained using the G3MP2//B3LYP energies, whereas the dashed lines are obtained using the RCCSD(T)/CBS energies. Note that the total rate coefficients do not change with the levels of theory. The total rate coefficients for the $C_2H_3 + O_2$ reaction (ref 17a) are also shown in the figure for comparison.

The temperature dependence of the rate coefficients was calculated in the range 200−2000 K and in the helium pressure of 2 Torr. The results are shown in Figure 5. The first important conclusion is that the theoretically predicted total rate coefficients are in good agreement with the available experimental data.[4] Second, the total rate coefficients exhibit strong negative temperature dependence. From 200 to 2000 K, the total rate coefficients decrease by nearly an order of magnitude. Third, the total rate coefficients are independent of the relative

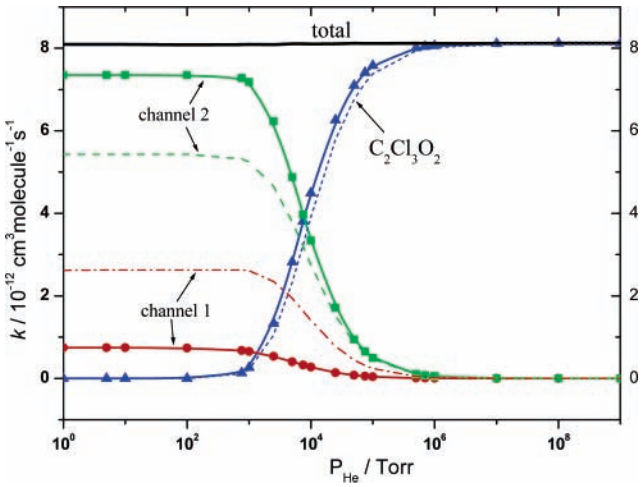

Figure 6. The pressure dependence of the calculated total rate coefficients and the individual rate coefficients for the channels 1 and 2 (at 297 K) and for the deactivation of the $C_2Cl_3O_2$ adduct. The solid lines are obtained using the G3MP2//B3LYP energies, whereas the dashed lines are obtained using the RCCSD(T)/CBS energies.

importance of TS1 and TS2. As mentioned above, the energy difference (ΔE_a) between TS1 and TS2 varies dramatically with the levels of theory. At the G3MP2//B3LYP level, $\Delta E_a = 28$ kJ/mol in contrast to $\Delta E_a = 6$ kJ/mol at the RCCSD(T)/CBS//CCSD level. As a result, the relative branching ratios for the two channels change dramatically as shown in Figure 5. However, it is clear that the channel 1 is always predominant over the channel 2. For the $O(^3P) + C_2Cl_3O$ channel, if the G3MP2//B3LYP energies are used, the rate coefficients are only weakly temperature dependent. If the RCCSD(T)/CBS//CCSD energies are used, the rate coefficients show strong negative temperature dependence. Although the RCCSD(T)/CBS//CCSD data should be more reliable than the G3MP2//B3LYP data, the experimental measurement on the $O(^3P) + C_2Cl_3O$ channel is necessary to support the theoretical result. In fact, the production of $O(^3P)$ atoms in the $C_2Cl_3 + O_2$ reaction has never been reported. We are expecting that the current theoretical study can invoke experimental investigation on the $O(^3P)$ production in the $C_2Cl_3 + O_2$ reaction and on the yield measurements.

For practical use, the temperature-dependent total rate coefficients were fitted by an empirical three-parameter expression as follows:

$$k(T) = 3.86 \times 10^{-12}\ \text{cm}^3\text{molecule}^{-1}\text{s}^{-1}\ (T/298)^{-0.474} \exp(224/T),$$

for $T = 200-2000$ K.

The pressure dependence of the rate coefficients was studied at $T = 297$ K, and the results are shown in Figure 6. A few important results can be obtained straightforwardly. First, the total rate coefficients are almost independent of the pressures in the range $1-10^9$ Torr. Experimentally there is no pressure dependence observed, which could confirm the present theoretical results. In fact, in the pressure range 1−2 Torr used in RSGS's experiments,[4] the deactivation of the initial adduct ($C_2Cl_3O_2$, IM1t) is negligible. The deactivation of IM1t is significant only at pressures higher than 1000 Torr. At about 10^4 Torr (ca. 13 atms), the three channels listed in the figure have similar rate coefficients. Second, the individual rate coefficients show typical "*S*" falloff behavior. Third, the relative importance of the product channels via TS1 and TS2 depends on the levels of theory, but the yield of $C_2Cl_3O_2$ is only slightly changed. Additionally, although the individual rate coefficients can change more or less with the different energy transfer parameters, the basic features of the pressure dependence of the rate coefficients are not sensitive to the energy transfer parameter.

The overall reaction is a typical "capture limited" process, that is, the total rate coefficients are predominantly determined by the energetics of the entrance regardless of the existence of the multiple exit barriers. The redissociation of IM1 back to the initial reactants is very slow and thus negligible in comparison with the subsequent low-barrier exit reaction to the final products. As a result, the overall reaction proceeds forward exclusively on the attractive entrance potential energy surface and acts as a simple $C_2Cl_3 + O_2 \rightarrow$ products bimolecular reaction. Therefore, the total rate coefficients are independent of the TS1 or TS2 and appear to be pressure independent.

4. The Chlorination Effect. It is interesting to compare the $C_2Cl_3 + O_2$ reaction with the $C_2H_3 + O_2$ reaction and thus to know the influence of full chlorination of the vinyl radical on its reactivity. Theoretically the $C_2H_3 + O_2$ reaction has been calculated by Mebel, Diau, Lin, and Morokuma[17a] at the G2M-(RCC, MP2) level of theory which is similar to the present G3MP2 method. Moreover, the geometries of the stationary points were also optimized at the B3LYP/6-311G(d,p) level of theory. Recently, the dominant reaction routes in the $C_2H_3 + O_2$ reaction were recalculated by Mebel and Kislov[17b] at the RCCSD(T)/CBS level and MRCI level of theory. The comparisons between the geometries of some stationary points are shown in Figures 2 and 3. The corresponding energies are compared in Table 1 (see the data in brackets).

It is not surprised that the $C_2Cl_3 + O_2$ reaction has the similar mechanisms with the $C_2H_3 + O_2$ reaction. Moreover, the dominant product channels are also the same, e.g., three-member-ring path and the OO bond cleavage path for both reactions. Of course some differences do exist in view of the barrier heights and the well depths of the intermediates. For example, although the geometrical parameters of the entrance intermediate (IM1t) are almost identical, the energy of IM1t in the $C_2Cl_3 + O_2$ reaction is about 40 kJ/mol shallower than that in the $C_2H_3 + O_2$ reaction. However, the other intermediates, IM2 and IM4, have the similar energies and the similar geometries. The barriers for TS1 and TS2 are both lowered due to the chlorination. With respect to the reactants, the barrier for TS2 is −56 kJ/mol in the $C_2Cl_3 + O_2$ reaction, in comparison with the value of −28 kJ/mol in the $C_2H_3 + O_2$ reaction. It is worth noting that the chlorination has a significant impact on the transition state TS3. In view of the geometrical parameters, the breaking OO bond of TS3 becomes shorter (ca. 0.1 Å) and the forming OC bond distance becomes longer (ca. 0.15 Å); in view of energies, the barrier for TS3 is lowered dramatically by about 55 kJ/mol. Therefore, the relative order of TS1 (ring forming) and TS3 (ring open) is changed. In the $C_2H_3 + O_2$ reaction, TS3 is slightly higher than TS1. In the $C_2Cl_3 + O_2$ reaction, TS3 does not play any role because it is much lower than TS1. It is indicated that the chlorination makes the three-member-ring COO structure of IM2 less stable.

The chlorination affects the reaction thermochemistry as well. For example, the $ClCO + CCl_2O$ channel is exothermic by 476 kJ/mol, in comparison with the exothermicity of 392 kJ/mol for the analogous $HCO + CH_2O$ channel. The $Cl + (ClCO)_2$ channel is exothermic by 443 kJ/mol, in comparison with the exothermicity of 322 kJ/mol for the $H + (HCO)_2$ channel. Moreover, a few exothermic channels in the $C_2H_3 + O_2$ reaction such as $C_2H_2 + HO_2$ become endothermic in the $C_2Cl_3 + O_2$ reaction. Interestingly, the exothermicity of the CO_2 production

channel is almost unaffected (e.g., −560 kJ/mol for $CO_2 + CCl_3$ vs. −566 kJ/mol for $CO_2 + CH_3$).

Concerning the rate coefficients, it is obvious that the chlorination makes the reaction slower by about a factor of 2 (see Figure 5) because of the slower capture rate for the association of O_2 with the heavy C_2Cl_3 radical. However, the total rate coefficients of both reactions have the negative temperature dependence. Moreover, no pressure dependence has been observed for both reactions.

IV. Conclusions

Using high-level ab initio theory, it is revealed that the $C_2Cl_3 + O_2$ reaction takes place via the barrierless addition/elimination mechanisms. The addition leads to the formation of the chlorinated vinylperoxy radical. The three-member-ring reaction path is the most favorable mechanism, leading to many highly exothermic products including $ClCO + CCl_2O$, $CO_2 + CCl_3$, $CO + CCl_3O$, $Cl + (ClCO)_2$, etc. The simple OO bond cleavage mechanism, leading to the formation of atomic oxygen $O(^3P)$ and C_2Cl_3O, can be competitive with the three-member-ring mechanism. The rest of mechanisms including four-member-ring paths are unimportant.

Kinetically, the total rate coefficients of the $C_2Cl_3 + O_2$ reaction show the negative temperature dependence in the range 200−2000 K and almost have no pressure dependence at 297 K. The individual rate coefficients for the three-member-ring reaction and for the $O(^3P)$ production depends strongly on the relative barrier heights of two key transition states, namely, TS1 (ring-forming) and TS2 (bond fission). Further experimental studies on the product distributions of the $C_2Cl_3 + O_2$ reaction should be interesting.

Acknowledgment. This work was supported by A Foundation for the Author of National Excellent Doctoral Dissertation of PR China (FANEDD, 200224) and by the Scientific Research Foundation for the Returned Overseas Chinese Scholars, State Education Ministry.

References and Notes

(1) Senkan, S. M.; Robinson, J. M.; Gupta, A. K. *Combust. Flame* **1983**, *49*, 305.

(2) Chang, W. D.; Karra, S.; Senkan, S. M. *Combust. Sci. Technol.* **1986**, *49*, 107.

(3) Wang, H.; Frenklach, M. *J. Phys. Chem.* **1994**, *98*, 11465.

(4) Russell, J. J.; Seetula, J. A.; Gutman, D.; Senkan, S. M. *J. Phys. Chem.* **1989**, *93*, 1935.

(5) Su, H.; Kong, F. Private communications.

(6) (a) Becke, A. D. *J. Chem. Phys.* **1993**, *98*, 5648. (b) Lee, C.; Yang, W.; Parr, R. G. *Phys. Rev. B: Condens. Matter Mater. Phys.* **1988**, *37*, 785.

(7) Gonzalez, C.; Schlegel, H. B. *J. Phys. Chem.* **1989**, *90*, 2154.

(8) Curtiss, L. A.; Redfern, P. C.; Raghavachari, K.; Rassolov, V.; Pople, J. A. *J. Chem. Phys.* **1999**, *110*, 4703.

(9) Bartlett, R. J.; Purvis, G. D. *Int. J. Quantum Chem.* **1978**, *14*, 516.

(10) (a) Cizek, J. *Adv. Chem. Phys.* **1969**, *14*, 35. (b) Purvis, G. D.; Bartlett, R. J. *J. Chem. Phys.* **1982**, *76*, 1910. (c) Scuseria, G. E.; Janssen, C. L.; Schaefer, H. F., III. *J. Chem. Phys.* **1988**, *89*, 7382.

(11) Woon, D. E.; Dunning, T. H., Jr. *J. Chem. Phys.* **1993**, *98*, 1358.

(12) Knowles, P. J.; Hampel, C.; Werner, H.-J. *J. Chem. Phys.* **1993**, *99*, 5219

(13) (a) Feller, D. *J. Chem. Phys.* **1992**, *96*, 6104. (b) Helgaker, T.; Klopper, W.; Koch, H.; Noga, J. *J. Chem. Phys.* **1997**, *106*, 9639.

(14) Dunning, T. H., Jr.; Peterson, K. A.; Wilson, A. K. *J. Chem. Phys.* **2001**, *114*, 9244.

(15) Frisch, M. J.; Trucks, G. W.; Schlegel, H. B.; Scuseria, G. E.; Robb, M. A.; Cheeseman, J. R.; Montgomery, J. A., Jr.; Vreven, T.; Kudin, K. N.; Burant, J. C.; Millam, J. M.; Iyengar, S. S.; Tomasi, J.; Barone, V.; Mennucci, B.; Cossi, M.; Scalmani, G.; Rega, N.; Petersson, G. A.; Nakatsuji, H.; Hada, M.; Ehara, M.; Toyota, K.; Fukuda, R.; Hasegawa, J.; Ishida, M.; Nakajima, T.; Honda, Y.; Kitao, O.; Nakai, H.; Klene, M.; Li, X.; Knox, J. E.; Hratchian, H. P.; Cross, J. B.; Bakken, V.; Adamo, C.; Jaramillo, J.; Gomperts, R.; Stratmann, R. E.; Yazyev, O.; Austin, A. J.; Cammi, R.; Pomelli, C.; Ochterski, J. W.; Ayala, P. Y.; Morokuma, K.; Voth, G. A.; Salvador, P.; Dannenberg, J. J.; Zakrzewski, V. G.; Dapprich, S.; Daniels, A. D.; Strain, M. C.; Farkas, O.; Malick, D. K.; Rabuck, A. D.; Raghavachari, K.; Foresman, J. B.; Ortiz, J. V.; Cui, Q.; Baboul, A. G.; Clifford, S.; Cioslowski, J.; Stefanov, B. B.; Liu, G.; Liashenko, A.; Piskorz, P.; Komaromi, I.; Martin, R. L.; Fox, D. J.; Keith, T.; Al-Laham, M. A.; Peng, C. Y.; Nanayakkara, A.; Challacombe, M.; Gill, P. M. W.; Johnson, B.; Chen, W.; Wong, M. W.; Gonzalez, C.; Pople, J. A. *Gaussian 03*, revision B.05; Gaussian, Inc.: Pittsburgh, PA, 2003.

(16) Werner, H.-J.; et al. MOLPRO, version 2002.6.

(17) (a) Mebel, A. M.; Diau, E. W. G.; Lin, M. C.; Morokuma, K. *J. Am. Chem. Soc.* **1996**, *118*, 9759. (b) Mebel, A. M.; Kislov, V. V. *J. Phys. Chem. A* **2005**, *109*,2005.

(18) Donaldson, D. J.; Okuda, I. V.; Sloan, J. *J. Chem. Phys.* **1995**, *193*, 37.

(19) (a) Klippenstein, S. J.; et al. VARIFLEX: version1.00, 1999. (b) Wardlaw, D. M.; Marcus, R. A. *Chem. Phys. Lett.* **1984**, *110*, 230. (c) Klippenstein, S. J. *J. Phys. Chem.* **1994**, *98*, 11459.